Published in J. Vac. Sci. Technol. B 15, 1027 (1997).

Morphological and compositional variations in strain-compensated InGaAsP/InGaP superlattices

R.S. Goldman[(a)] and R.M. Feenstra[(b)]
Department of Physics, Carnegie Mellon University, Pittsburgh, Pennsylvania 15213
C. Silfvenius, B. Stålnacke, and G. Landgren
Department of Electronics, Royal Institute of Technology, Kista, Sweden

Abstract

We have investigated the properties of strain-compensated InGaAsP/InGaP superlattices, grown by metalorganic vapor phase epitaxy, with and without InP interlayers inserted in the InGaP barrier. Using cross-sectional scanning tunneling microscopy and spectroscopy, we observe lateral variations in layer thickness and electronic properties. When the number of superlattice periods is increased from 8 to 16, the surface develops large undulations in the top 2–4 superlattice periods. This occurs simultaneously with reduced PL efficiency. For structures with InP layers inserted in the InGaP barrier, only slight undulations of the top superlattice periods occur, and the PL is significantly improved. We discuss the origins of the surface undulations in terms of a model which relates their formation with the elastic relaxation of strain arising from thickness and/or composition variations in the superlattice layers. Finally, we observe a 4-fold periodicity of the (001) lattice planes, presumably arising from atomic ordering in the alloys.

1 Introduction

InGaAsP-based multiple quantum well structures with alternating compressive- and tensile-strained layers are promising for optoelectronic device applications, such as light sources and detectors in optical fiber communications systems.[1] Although the structures are intended to be strain-balanced, the optical properties are often degraded by residual-strain related effects.[2] In particular, lateral variations in surface morphology and/or alloy composition have been observed.[3,4] The interplay between these phenomena, and their effects on optical properties are not well understood. A detailed study of the nanometer-scale structure and electronic properties is essential for understanding the residual-strain related effects and their impact on PL efficiency.

In this paper, we present cross-sectional scanning tunneling microscopy (STM) and spectroscopy studies of a series of InGaAsP/InGaP superlattices produced by metalorganic vapor phase epitaxy (MOVPE). The structures have an effective bandgap around 1.3 μm and have a constant In/Ga ratio in both well and barrier. Apart from fabrication convenience this results in very deep electron wells, thereby minimizing the carrier leakage which is a major problem in many 1.3 μm laser designs leading to poor high temperature performance. In some of the superlattices we find lateral variations in the effective band gaps and layer thicknesses of the ternary and quaternary alloy layers. In addition, we observe surface undulations whose amplitude depends on the total num-

ber of superlattice periods and the presence of InP interlayers in the InGaP barrier. Furthermore, the photoluminescence (PL) efficiency of the structures is qualitatively dependent on the amplitude of the surface undulations. In some cases, we find a 4-fold periodicity of the (001) planes, presumed to arise from atomic ordering of the alloys. We discuss the origins of the surface undulations in the context of a model relating their formation with elastic relaxation of strain arising from thickness and/or composition variations in the superlattices.

The paper is organized as follows. Section 2 describes the experimental details, including growth conditions and characterization by x-ray diffraction and photoluminescence. STM images and spectroscopy data, as well as a model illustrating the structural degradation process, are presented in section 3 . Finally, conclusions are given in section 4 .

2 Experimental Details

The samples were prepared by MOVPE at a pressure of 50 mbar, using trimethylindium (TMI), trimethylgallium (TMGa), AsH_3, and PH_3 as source gases. The undoped structures were grown on sulfur-doped (N_d=5 x 10^{18} cm^{-3}) InP substrates, at a substrate temperature of 680° C.[2] The targeted structures included 8 or 16 period superlattices (multi-quantum wells) surrounded by a 240 nm InP buffer layer and 150 nm InP cap. Each superlattice period consisted of a quantum well of 5 nm $In_{0.89}Ga_{0.11}As_{0.55}P_{0.45}$ and a barrier of either 9 nm $In_{0.89}Ga_{0.11}P$ or 4.5 nm $In_{0.89}Ga_{0.11}P$ + 10 nm InP + 4.5 nm $In_{0.89}Ga_{0.11}P$. Since the quantum well and barrier have 1.0 % compressive and 0.8 % tensile lattice-mismatch strains, respectively, relative to the InP substrate, the strain is nearly balanced. In principle, it should be possible to grow multiple superlattice periods, without degradation of the optical properties. However, the measured 300 K photoluminescence (PL) intensities were highest and lowest for the 8- and 16-period superlattices, respectively, with intermediate values for the 16-period superlattices with InP interlayers.[2] High-resolution x-ray diffraction spectra showed higher satellite peak intensities for the 8-period than the 16-period superlattices, indicating a more well defined periodic structure in the 8-period superlattices. For the 16-period superlattices with InP interlayers in the InGaP barrier, the satellite peaks in the x-ray diffraction spectrum were also well defined, but direct comparison with the other two spectra is not straightforward. Although the x-ray results indicate a link between a less pronounced periodic structure and reduced PL efficiency, they do not provide detailed information about how the superlattice periodicity has been reduced.

For STM, the samples were cleaved to expose a $(\bar{1}10)$ surface, in an ultra-high-vacuum chamber with base pressure < 5 x 10^{-11} Torr. STM was performed with both electrochemically etched single crystal <111>-oriented W and commercially available Pt-Ir tips. The tips were cleaned by *in-situ* electron bombardment and characterized by *in-situ* field-emission microscopy. Images were obtained with a constant tunnel current of 0.1 nA, and sample bias voltages as described below. Details of the STM design,[5] cleavage procedure,[6] and spectroscopic methods[7] have been presented elsewhere.

3 Results and Discussion

Figures 1 (a) – (d) show large-scale STM topographic images of the 16-period InGaAsP/InGaP superlattices, displayed with the growth direction from right to left. In both empty and filled state images, Figs. 1(a) and (c) respectively, the InGaAsP (quaternary) and InGaP (ternary) layers appear

as alternating bright and dark layers sandwiched between thick layers of InP (the buffer and cap). Since the InGaAsP/InGaP system is a type I superlattice, both electrons and holes are confined in the InGaAsP layers. Thus, for a given tip-sample bias voltage in the STM, a greater number of filled or empty states contribute to the tunnel current for the InGaAsP layers compared to the InGaP layers. In order to maintain a constant tunneling current, the tip moves towards the surface in the vicinity of the InGaP, and away from the surface in the vicinity of the InGaAsP. As a consequence, the InGaP and InGaAsP layers appear as dark and bright layers, respectively.

The images of Fig. 1 clearly reveal structural degradation of the superlattice layers. In particular, large surface undulations and large lateral variations in image contrast are apparent. These surface undulations arise from relaxation of strain accumulated in the superlattices during growth. The lateral variations in image contrast are due to a combination of band edge shifts due to varying thicknesses, alloy compositions, and strains in the layers, as well as a distortion of the surface associated with relaxation of strain during cleaving. These effects will be discussed in more detail below.

Figs. 2 (b) and (d) show topographic images in which the local background (formed by averaging the data over an area of 20×20 nm^2) has been subtracted from Figs. 2 (a) and (c), respectively. In Figs. 2 (b) and (d), much of the lateral image contrast variation is suppressed, such that lateral variations in the layer thicknesses are evident. The observed structural degradation process is divided into two regimes: phase I – where the superlattice period is conserved, and phase II – where the superlattice period varies and large undulations of the surface occur. We note in particular that in the phase I region significant changes in layer thickness are observed, as seen most clearly in filled state images such as Fig. 1(d), with thin quaternary layers and thick ternary layers (the sum of their thicknesses is fixed). Closest to the substrate is region Q+T, where the superlattice layer thicknesses are fixed at the targeted values. In Fig. 2 (a), we present a high-resolution view of region Q+T, acquired at a sample bias voltage of +2.5 V. Fringes with a spacing of 5.8 and 5.9 Å, corresponding to the (001) planes of the ternary and quaternary alloys, are observed in the dark and bright layers, respectively. The image consists primarily of three superlattice periods, with typical ternary and quaternary thicknesses 10.0 and 4.7 nm, close to the targeted values.

Additional regions denoted in Figs. 1 (b) and (d) are q'+T', with thin quaternary and thick ternary layers, and Q'+t', with thick quaternary and thin ternary layers. In both cases, the primes indicate a possible change in alloy composition in the layers. The thickness variations are most evident in the close-up views shown in Figs. 2 (b) and (c), acquired at sample bias voltages -1.8 and +1.8 V, respectively. Fig. 2 (b) displays a close-up view of a (growth front) morphological undulation, where the top 5 superlattice periods in regions q'+T' and Q'+t' (phase II) are displayed. Lateral variations in the ternary and quaternary layer thicknesses are evident. In Fig. 2 (c), we show a high resolution view of region Q'+t' (also phase II). Similar to Fig. 2 (a), fringes corresponding to the (001) planes of the ternary and quaternary alloys are observed. The image consists of 2 superlattice periods, with ternary layers as thin as 1.2 nm. It is evident from this image that the (001) lattice planes remain aligned along the [110] direction while the profiles of the ternary and quaternary layers do not. This indicates a change in surface normal during the growth of the undulations (*i.e.* faceting), similar to that reported in InGaP/InAsP structures.[3]

Some of the accumulated strain in the 16-period superlattices is probably relaxed elastically

by the formation of the observed surface undulations. In addition, the elastic relaxation in some cases is accompanied by plastic relaxation, as we see in the image in Fig. 3 . In this empty state image, acquired at a sample bias voltage of +2.5 V, a surface step extending out from the cusp in the valley is observed. We attribute this step to a screw-type dislocation occurring near the cusp of the valley. We cannot say at present whether the dislocation was nucleated before the valley formed (*i.e.* due to high stress at the cusp), or alternatively, that the dislocation formed first and its associated stress relaxation produced a large variation in growth rates which then led to the valley formation. In either case however, the existence of the dislocation is a clear indication of the high stress levels in the region near the cusp of the valley.

In order to quantify the lateral band gap variations observed in bias-dependent topography images, we performed spatially-resolved spectroscopy measurements in the different regions outlined in Fig. 1 (b) and (d). In Fig. 4 , the normalized conductance versus sample bias voltage are plotted for (a) the quaternary layers, (b) the ternary layers, and (c) the InP substrate or cap layers. For each layer, the normalized conductance versus sample bias voltage was collected in the Q+T, Q'+t', and q'+T' regions (the InP spectra were acquired *nearby* those labeled regions). All the spectra display well defined band edges, as marked by dashed lines in Fig. 4. The nonzero conductance observed within the gap is the "dopant-induced" component, which arises from electrons tunneling out of filled conduction band states.[7] The results of the gap measurements are summarized in Table I. As mentioned earlier, the InGaAsP/InGaP system is a type I superlattice, with both electrons and holes confined in the InGaAsP (quaternary). Therefore, the effective band gap of the ternary corresponds to the energy difference between the InGaP conduction band edge and InGaP light hole valence band, while the effective band gap of the quaternary corresponds to the energy difference between the first electron (e_0) and first hole (h_0) subbands ($E_{e0\text{-}h0}$) in the InGaAsP.

We have calculated the expected effective band gaps of the ternary and quaternary layers of the superlattice, taking into account the lattice mismatch strain, and possible variations in layer thickness and/or alloy compositions. Strain effects are included assuming biaxial strain and using the appropriate deformation potentials [8], and subband energies are computed using the transfer matrix method [9]. Results are shown in Table I. For region Q+T, with ternary and quaternary alloy compositions and layer thickness fixed at the targeted values, the calculated effective band gaps of the ternary and quaternary are 1.41 and 0.94 eV, respectively. These values are within the error of our measured values, 1.50 ± 0.10 and 1.05 ± 0.10 eV for the ternary and quaternary, respectively. In region q'+T', with thick ternary and thin quaternary layers, the calculated effective band gaps of the ternary and quaternary are 1.41 and 1.13 eV, respectively. In this case, the calculated quaternary band gap is within the error measured value, 1.20 ± 0.10 eV, but the calculated ternary band gap is smaller than our measured value, 1.56 ± 0.10 eV. Thus, additional factors, such as composition variations and/or lateral strain variations (non-biaxial strain) may contribute to the larger measured effective gap. If we consider a composition variation of +5% Ga ($In_{0.84}Ga_{0.16}P$), the calculated effective band gap of the ternary is slightly increased to 1.44 eV which is closer to our measured value discussed above. Additional contributions due to non-biaxial strain will be discussed below. The calculated effective band gaps for the ternary and quaternary in region Q'+t' are 1.41 and 0.88 eV, respectively. Similar to region q'+T', the calculated effective gap of the quaternary is within the error of our measured value, 0.90 ± 0.10 eV, but that of the ternary is larger than our measured value, 1.28 ± 0.10 eV. If we consider a composition variation of -5% Ga ($In_{0.94}Ga_{0.06}P$), the calculated effective band gap of the ternary is decreased to 1.38 eV, which is within the error

of the measured value.

Considering now the effects of lateral strain variations (non-biaxial strain) on the observed bands gaps, it is clear that in the q'+T' region there will be additional tensile strain due to the larger amount of ternary (small lattice constant) material. If we approximate the q'+T' material as being composed *entirely* of ternary material T', with mismatch $f = (a_{InP} - a_{InGaP}) / a_{InGaP} = +0.0079$, and further consider this region to be a spherical inclusion embedded in InP, then the strain in the inclusion can be computed using an analytic solution for the elasticity equations for this geometry.[10] Computing band edge shifts using the appropriate deformation potentials, [8] we find that the band gap of the T' region will be reduced by 0.050 eV compared with bulk $In_{0.89}Ga_{0.11}P$. This value must be compared with the expected gap of the ternary material in the Q+T region, which is under biaxial strain leading to a band gap reduction of 0.101 eV. Thus, the net effect is an *increase* of the ternary gap in the q'+T' material of about 0.05 eV compared to that in Q+T, which leads to better agreement between the theory and observed gap energies. Considering the thin quaternary layers in the q'+T' regions to be biaxially strained onto the T' material leads to only an 0.01 eV increase in their band gap compared to the Q+T material. Finally, for the Q'+t' region, the strain is somewhat uncertain due to observed dislocation formation, so we do not attempt any further corrections to those band gap estimates.

In summary, the data indicate 0.1-0.2 eV variations in the effective band gaps of both the ternary and quaternary alloys, in the Q+T, Q'+t', and q'+T' regions. For imaging voltages with magnitude gta 2 V, this amount of band edge shift would lead to variations in tip-sample spacing of lta 1 Å, which is much less than the 10 Å contrast variation observed in the constant-current images of Fig. 1(a) and (c). Other electronic effects such as tip-induced band bending could conceivably play a role in producing these large contrast variations. However, another effect to consider, which is purely topographic (non-electronic) in origin, is the influence of strain relaxation of the cleavage surface itself. This effect has been previously suggested by Pinnington *et al.* in their study of Si/Ge heterostructures.[11] In our case, the q'+T' layers have additional tensile strain compared to the Q+T region as discussed above, and similarly the Q'+t' region is expected to have additional compressive strain. Thus, when the sample is cleaved, these regions will relax inwards and outwards, respectively, from the cleavage face, in agreement with the observed sign of the contrast in Fig. 1.

When InP interlayers are inserted in the InGaP barrier, the structural degradation is greatly reduced. In Fig. 5 (a) and 5 (b), we present large-area topographic and conductance (dI/dV) images of 16-period superlattices with InP interlayers inserted in the InGaP barrier. The images are displayed with the growth direction from right to left, and the y-scale is compressed by a factor of 2.5. In the empty state topographic image presented in Fig. 5 (a), acquired at a sample bias voltage of +2.5 V, a sequence of dark, bright, dark, and medium layers, corresponding to the ternary, quaternary, ternary, and InP, is sandwiched between an InP buffer and cap layers. The image also reveals lateral contrast variations similar to the superlattices without InP interlayers (as in Figs. 1 (a) and 1 (c)). Thickness variations in the ternary and quaternary layers are most evident in the conductance image shown in Fig. 5 (b). In this case, only slight undulations of the top superlattice period are observed. Evidently, the build-up of strain at the growing surface is reduced by the InP interlayers.

We have shown several images illustrating lateral variations in layer thickness, effective

band gap, and surface morphology in InGaAsP/InGaP superlattices. Here, we present a model relating the degradation of the structures with the build-up of strain in the superlattices. In phase I, shown in Fig. 6 (a), the process begins with the random formation of a thin region of a quaternary layer. Deposition of the next ternary layer will produce a strain variation at the surface due to the quaternary layer thickness variation.[12,13] Assuming that the growth rate depends on strain, the resulting more negative (compressive) in-plane strain would favor the attachment of small atoms.[14] In this case, the strain variation will inhibit further quaternary growth and favor ternary growth. Thus, a region with thin quaternary and thick ternary layers (q'+T') is formed. This region propagates and grows in size laterally as more layers are deposited. Alloy composition variations may also occur, with Ga and/or P-rich q'+T' regions (indeed, we cannot distinguish between a random variation in thickness or composition which acts to nucleate the degradation process). Similar effects have been observed in InGaP/InAsP[3] and Si/Ge[15] superlattices. As the process shown in Fig. 6 (a) continues, the lateral inhomogeneities in layer thickness and possible compositional variations will increase, leading to large lateral variations in the strain of the layers. This accumulated lateral strain then begins to relax elastically and/or plastically in phase II.

Phase II of the degradation process is characterized by a superlattice period which is no longer fixed. Deep valleys form in the morphology. The resulting surface undulations may act to relieve stress (elastic relaxation), and, in addition, dislocations are observed to form near the cusps of the valleys (plastic relaxation). The Q'+t' regions forming near the valleys have very thin ternary layers. As in phase I, we associate this change in layer thickness with a reduced growth rate, due in this case to additional tensile in-plane strain in this region. This strain may also induce alloy compositional variations in this region. For the superlattices grown with InP interlayers, the propagation of strain build-up in the structure is slowed due to additional strain balancing from the InP. Furthermore, the propagation of alloy composition variations through the structure is filtered by the InP interlayers, due to the lack of alloy decomposition in a binary alloy. The superlattices with InP interlayers have remained in phase I of the process, and the size of the thickness and/or composition modulated regions is limited. Based on this model, we predict that it will be possible to grow many more periods of superlattices with InP interlayers without degradation of the structure.

In addition to the lateral variations in layer thickness and effective band gap, and surface morphology, in some regions we observe a multiplicity in the atomic periodicity, as displayed in Fig. 7 . That image shows the top 6–7 superlattice periods, in the vicinity of a valley and nearby hill of an undulation, acquired at a sample bias voltage of +2.5 V. Lateral variations in layer thicknesses are observed, as discussed in Figs. 1 – 3 . In addition, fringes with a spacing of 24 Å, are evident. Similar to the lattice planes in Fig. 2 , the fringes remain aligned along the [110] direction while the profiles of the ternary and quaternary layers do not. This periodicity corresponds to a 4-fold multiple of the (001) atomic spacing, suggesting atomic ordering in the alloys. Although atomic ordering has been previously discussed in compound semiconductor alloys, [16] this 4-fold periodicity has not been previously reported. Furthermore, it is not explained by either CuPt or CuAu ordering, which would lead to a 2-fold multiple of the (001) atomic spacing.[16,17] As seen on the left-hand side of Fig. 7, the 4-fold periodicity extends into the overlaying InP layers, indicating a perturbation in the charge density of the InP. The charge density perturbation is probably enhanced by surface relaxation. The amplitude of this perturbation in the InP decays to zero at a distance of about 50 nm from the InGaP/InGaAsP superlattice. Further work is required to understand the origin of the 4-fold periodicity and its implications on the present models for ordering in compound

semiconductors.

4 Conclusions

We have investigated the properties of InGaAsP/InGaP superlattices, grown with or without InP layers inserted in the InGaP barriers. Spatially-resolved spectroscopy reveals variations in the effective band gaps of the superlattice layers. STM topography images indicate lateral variations in the layer thickness of the ternary and quaternary alloys of the superlattices. In some cases, we find a 4-fold periodicity of the (001) planes, presumed to arise from atomic ordering in the alloys. When the number of superlattice periods is increase from 8 to 16, the surface develops large undulations involving the top few superlattice periods. This effect is reduced in structures with InP layers inserted in the InGaP barrier. Furthermore, the PL efficiency increases with decreasing undulation amplitude. A model is presented describing the formation of the surface undulations in terms of accumulated strain due to the propagation of layer thickness and/or composition variations. Similar effects are expected to occur other strained-layer materials systems.

This work was supported in part by a grant from the National Science Foundation. Discussions with S. Mahajan, M. Skowronski, J. Tersoff, and T. Tiedje are gratefully acknowledged.

(*a*)Present address: Department of Materials Science and Engineering, The University of Michigan, Ann Arbor, Michigan 48109-2136. Electronic mail:rsgold@engin.umich.edu

(*b*)Electronic mail:feenstra@andrew.cmu.edu

[1] E.P. O'Reilly and A.R. Adams, IEEE J. Quantum Electronics **30**, 366 (1994).

[2] C. Silfvenius, B. Stålnacke, and G. Landgren, J. Cryst. Growth, in press.

[3] A. Ponchet, A. Rocher, A. Ougazzaden, and A. Mircea, J. Appl. Phys. **75**, 7881 (1994).

[4] G. Patriarche, A. Ougazzaden, and F. Glas, Appl. Phys. Lett. **69**, 2279 (1996).

[5] R.M. Feenstra, 21st Int. Conf. Phys. Semicond., ed. P. Jiang and H.-Z. Zheng (World Scientific, Singapore, 1992), p.357.

[6] R.M. Feenstra, E.T. Yu, J.M. Woodall, P.D. Kirchner, C.L. Lin, and G.D. Pettit, J. Vac. Sci. Technol. B **61**, 795 (1992).

[7] P. Mårtensson and R.M. Feenstra, Phys. Rev. B **39**, 7744 (1988); R. M. Feenstra, Phys. Rev. B **50**, 4561 (1994).

[8] C. G. Van de Walle, Phys. Rev. B **39**, 1871 (1989).

[9] B. Jonsson and S. T. Eng, J. Quantum Elec. **26**, 2025 (1990).

[10] R.S. Goldman, R.M. Feenstra, B.G. Briner, M.L. O'Steen, and R.J. Hauenstein, unpublished.

[11] T. Pinnington, A. Sanderson, T. Tiedje, T.P. Pearsall, E. Kasper, H. Presting, Thin Solid Films, **222**, 259 (1992).

[12] R.M. Feenstra and M.A. Lutz, J. Appl. Phys. **78**, 6091 (1995).

[13] J. Tersoff, C. Teichert, and M.G. Lagally, Phys. Rev. Lett. **76**, 1675 (1996).

[14] J.E. Guyer and P.W. Voorhees, Phys. Rev. B **54**, 1170 (1996).

[15] E. Carlino, L. Tapfer, and H. von Känel, Appl. Phys. Lett. **69**, 2546 (1996).

[16] See, for example, A. Zunger and S. Mahajan, in Handbook on Semiconductors, Vol. 3, ed. S. Mahajan (North-Holland, Amsterdam, 1994), p. 1399, and references therein.

[17] S. Froyen and A. Zunger, Phys. Rev. B **53**, 4570 (1996).

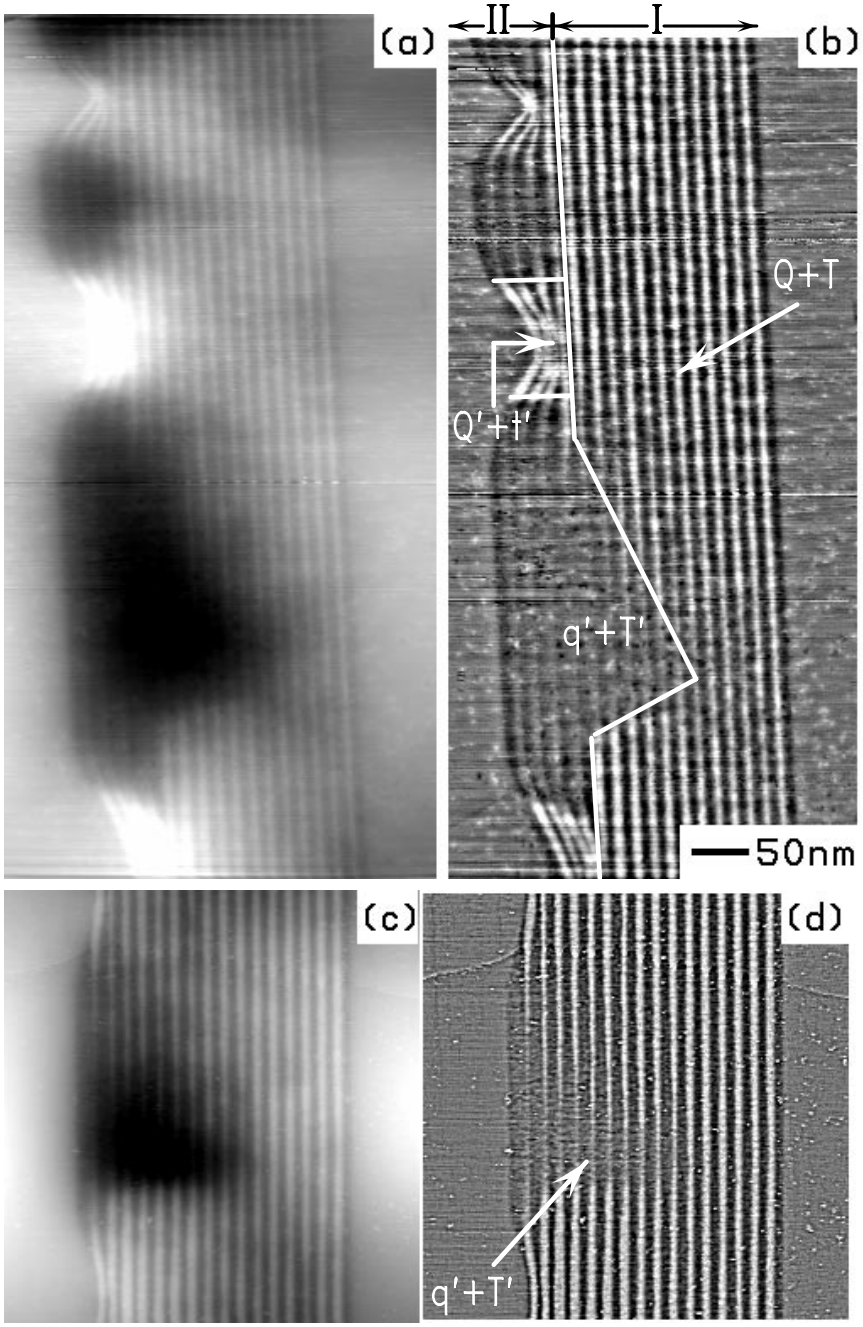

Figure 1 Large-scale topographic images of 16-period InGaAsP/InGaP superlattices, acquired at a sample bias voltages of (a),(b) +2.5 V and (c),(d) -2.0V. The InGaAsP (quaternary) and InGaP (ternary) layers appear bright and dark, respectively. The grey-scale ranges displayed are (a) 15 Å, (b) 1.7 Å, (c) 10 Å, and (d) 0.7 Å, where a local background subtraction was performed in (b) and (d).

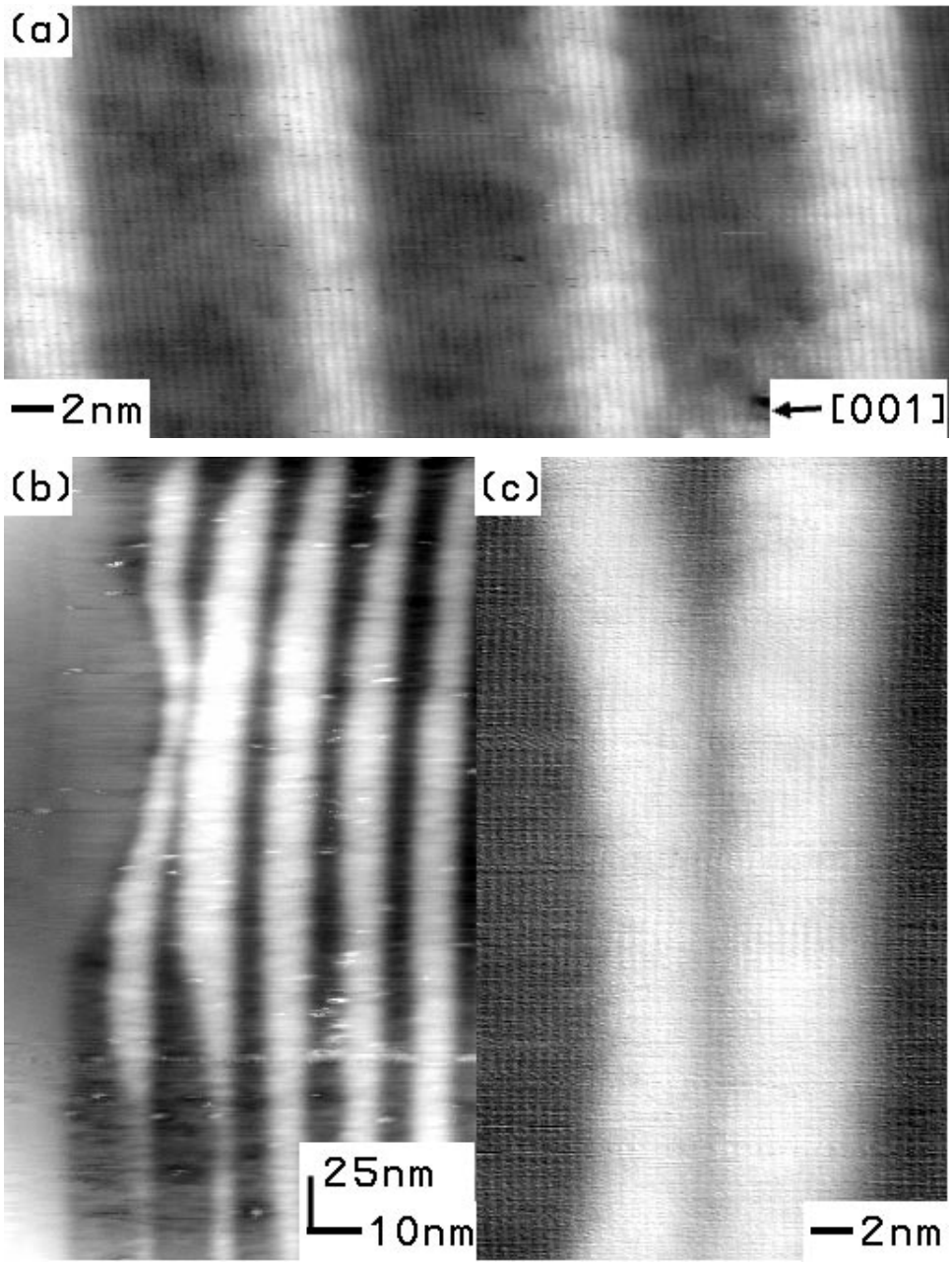

Figure 2 Close-up views of 16-period InGaAsP/InGaP superlattices. The high-resolution image of region Q + T displayed in (a), was acquired at a sample voltage of +2.5 V. The images in (b) and (c), acquired at sample voltages of -1.8 and +1.8 V, show a close-up view of an undulation, and a high-resolution view of region Q' + t'. The y-scale in (c) is compressed by a factor of 2.5

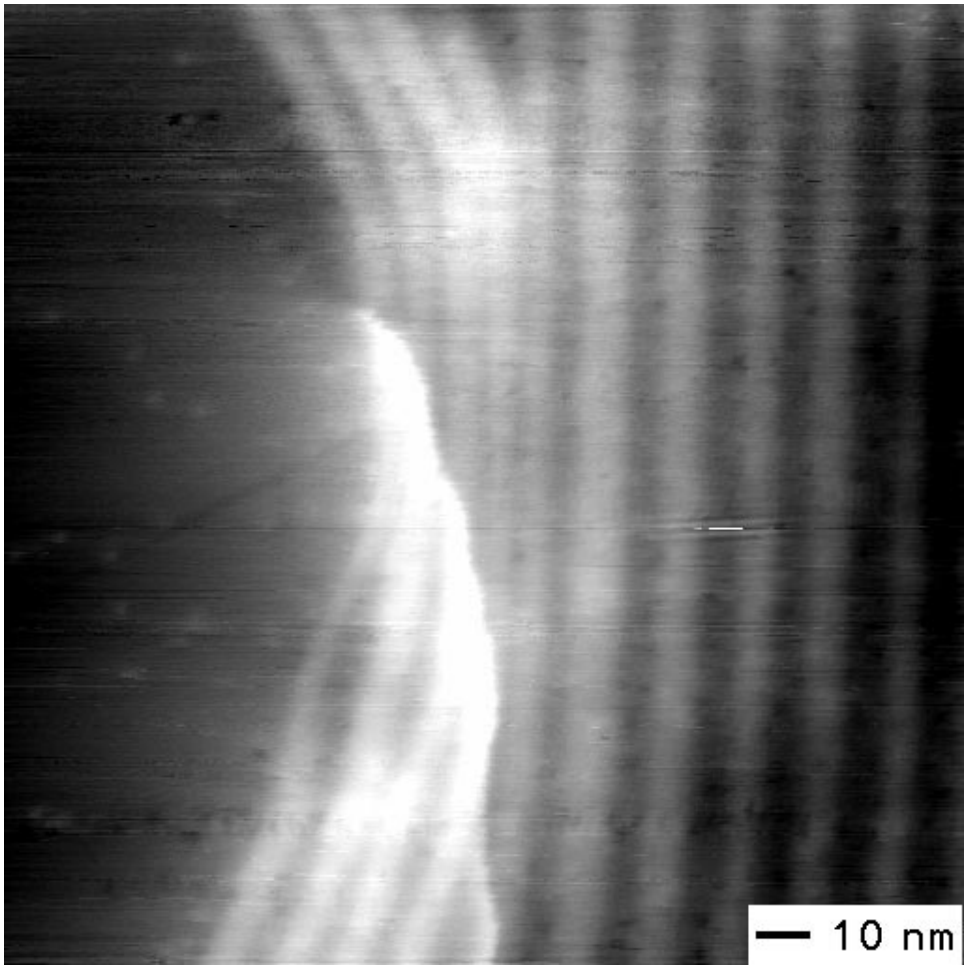

Figure 3 Topographic image acquired near a valley of an undulation, at a sample bias voltage of +2.5 V. A surface step extending out from the cusp in the valley is observed, and attributed to a dislocation.

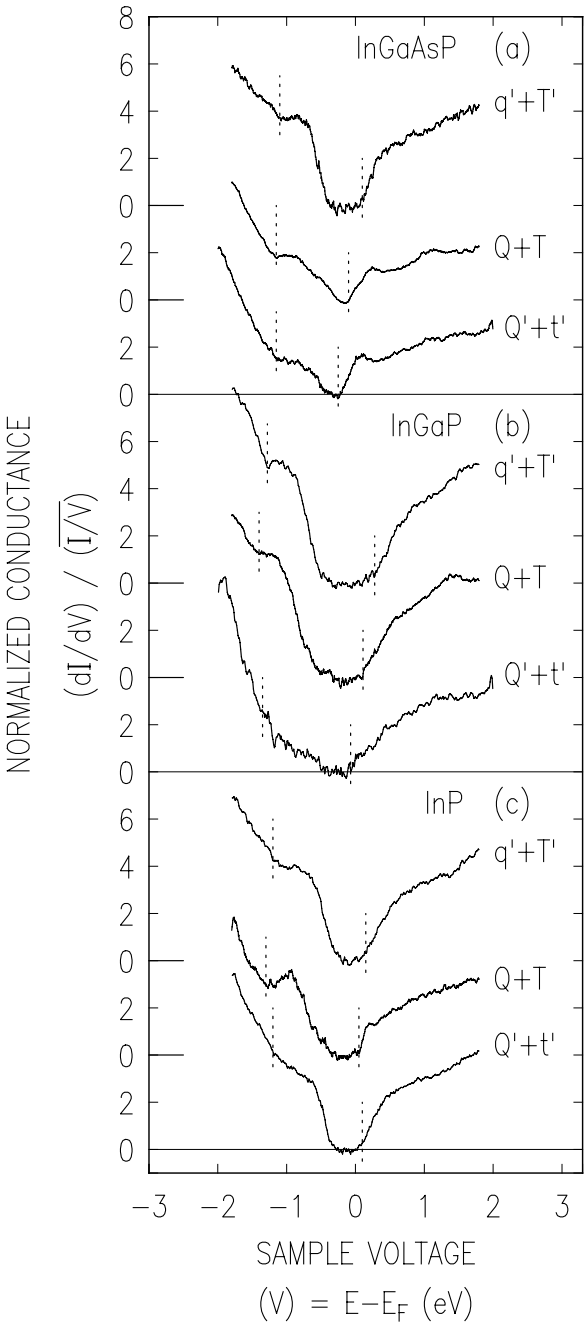

Figure 4 Spatially resolved spectroscopy results, acquired on the (a) quaternary layers, (b) ternary layers, and (c) on the InP substrate or cap layers. In each case, the location of the spectra in terms of the Q+T, Q'+t', or q'+T' regions is indicated (the InP spectra were acquired *nearby* those labeled regions.

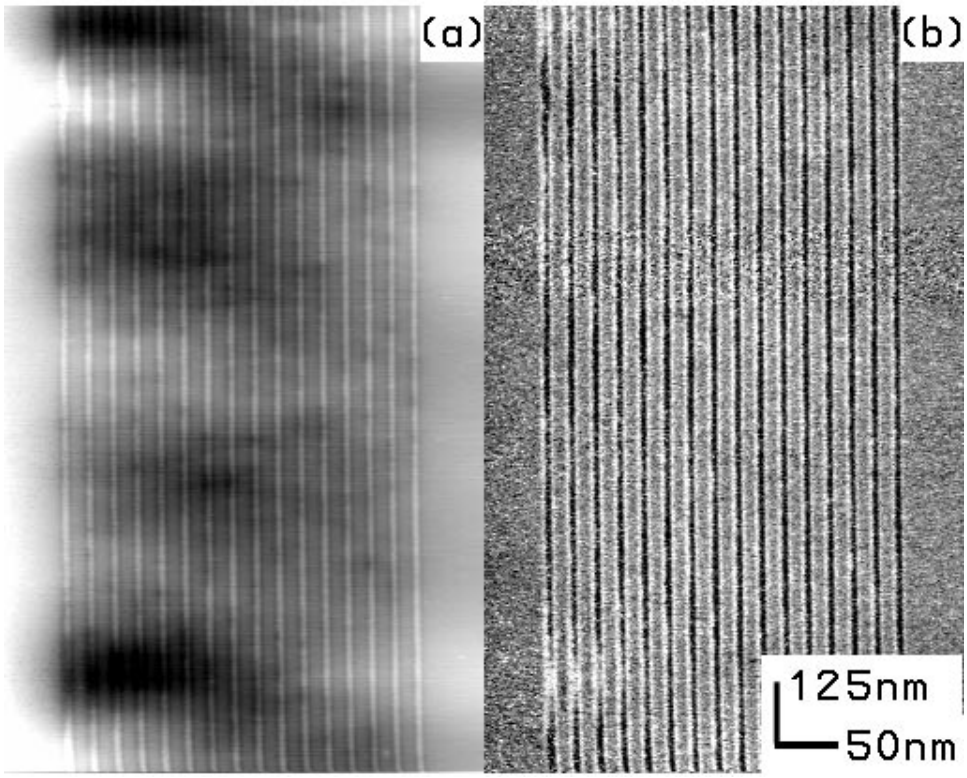

Figure 5 Large-area (a) topography and (b) conductance images of 16-period InGaAsP/InGaP superlattices, with InP interlayers inserted in the InGaP barriers, acquired at a sample bias voltage of +2.5 V. The y-scale in the images is compressed by a factor of 2.5. The grey-scale range displayed in (a) is 6.0 Å.

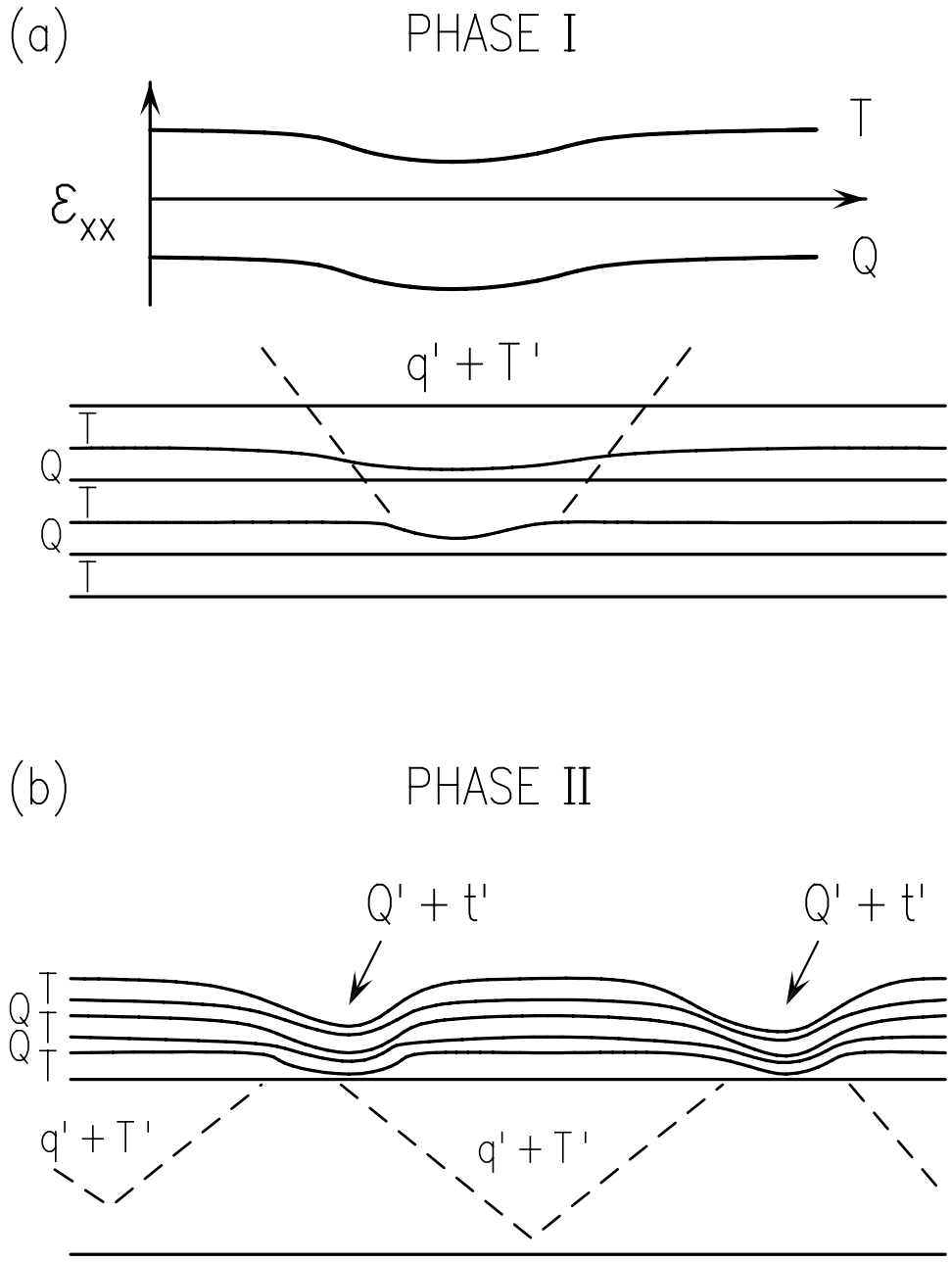

Figure 6 Model illustrating the build-up of strain in the degraded portions of the superlattice. In (a), the superlattice period is conserved (phase I). A quaternary layer (Q) which has a thin region is randomly formed. Deposition of the next ternary layer (T) will produce strain variations at the surface, due to the thickness variation of the quaternary layer. This region, denoted q'+T', propagates and grows in size laterally as more layers are deposited. As this process continues, lateral variations in strain will accumulate and at some point begin to relax. As shown in (b), the superlattice period then varies and large undulations of the surface develop (phase II), arising from a combination of elastic and plastic strain relaxation. Regions with thin ternary layers, Q'+t', are formed.

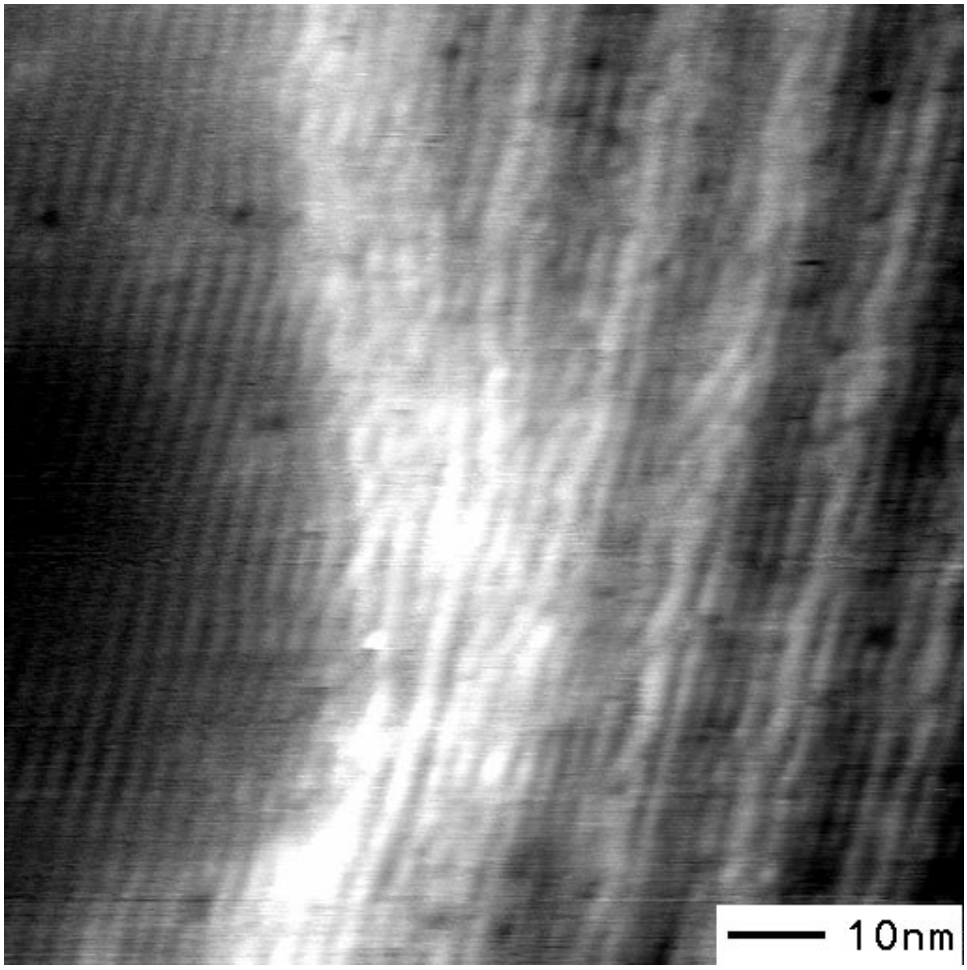

Figure 7 Topographic image of the top 6–7 superlattice periods, in the vicinity of a valley and nearby hill of an undulation, acquired at a sample bias voltage of +2.5 V. The grey-scale ranges displayed is 3.2 Å. Fringes with a spacing of 24 Å, corresponding to a 4-fold multiple of the (001) atomic spacing, are observed.